NIH Public Access
Author Manuscript
Nat Neurosci. Author manuscript; available in PMC 2015 February 01.

Published in final edited form as:
Nat Neurosci. 2014 August ; 17(8): 1130–1136. doi:10.1038/nn.3751.

Simultaneous transcranial magnetic stimulation and single neuron recording in alert non-human primates

Jerel K. Mueller[1], **Erinn M. Grigsby**[1,2], **Vincent Prevosto**[1], **Frank W. Petraglia III**[1], **Hrishikesh Rao**[1], **Zhi-De Deng**[3], **Angel V. Peterchev**[1,2,3,4], **Marc A. Sommer**[1,3,5,6], **Tobias Egner**[3,5,7], **Michael L. Platt**[3,5,6], and **Warren M. Grill**[*,1,2,3,6,8]

[1]Department of Biomedical Engineering, Duke University, Durham, NC 27708

[2]Department of Electrical and Computer Engineering, Duke University, Durham, NC 27708

[3]Department of Psychiatry and Behavioral Sciences, Duke University School of Medicine, Durham, NC 27710

[4]Duke Institute for Brain Sciences, Duke University, Durham, NC 27708

[5]Center for Cognitive Neuroscience, Duke University, Durham, NC 27708

[6]Department of Neurobiology, Duke University School of Medicine, Durham, NC 27708

[7]Department of Psychology & Neuroscience, Duke University, Durham, NC 27708

[8]Department of Surgery, Duke University School of Medicine, Durham, NC 27708

Abstract

Transcranial magnetic stimulation (TMS) is a widely used, noninvasive method for stimulating nervous tissue, yet its mechanisms of effect are poorly understood. Here we report novel methods for studying the influence of TMS on single neurons in the brain of alert non-human primates. We designed a TMS coil that focuses its effect near the tip of a recording electrode and recording electronics that enable direct acquisition of neuronal signals at the site of peak stimulus strength minimally perturbed by stimulation artifact in intact, awake monkeys (*Macaca mulatta*). We recorded action potentials within ~1 ms after 0.4 ms TMS pulses and observed changes in activity that differed significantly for active stimulation as compared to sham stimulation. The methodology is compatible with standard equipment in primate laboratories, allowing for easy implementation. Application of these new tools will facilitate the refinement of next generation TMS devices, experiments, and treatment protocols.

[*]to whom correspondence should be addressed: Department of Biomedical Engineering, Duke University, Box 90281, Durham NC 27708-0281, (919) 660-5276 PHONE, (919) 684-4488 FAX, warren.grill@duke.edu.

AUTHOR CONTRIBUTIONS

T.E., M.L.P, M.A.S., and W.M.G. designed the experiments. J.K.M., Z-D.D., A.V.P., and W.M.G. developed and constructed the TMS coil and associated electronics. Z-D.D., J.K.M., A.V.P., and W.M.G. conducted the modeling. V.P., F.W.P., J.K.M., E.M.G., H.R., and M.A.S. used the TMS technology in combination with neurophysiological techniques to collect and analyze the single neuron recording data in monkeys. J.K.M., M.A.S., and W.M.G. wrote the manuscript with editorial input from all of the other authors.

NIH-PA Author Manuscript
NIH-PA Author Manuscript
NIH-PA Author Manuscript

NIH-PA Author Manuscript

NIH-PA Author Manuscript

NIH-PA Author Manuscript

Transcranial magnetic stimulation (TMS) is a non-invasive method to activate the nervous system using an external coil to induce a brief, high intensity magnetic field[1]. TMS enables probing the relationship between activation of superficial neocortical areas and behavior. It is applied clinically to treat medication-resistant depression[2–4] and for presurgical cortical mapping[5]. Although TMS is in widespread use and continues to be investigated for multiple clinical applications including magnetic seizure therapy[6] and treatment of schizophrenia[7], there is limited understanding of the effects of TMS on neurons[8,9]. Improved understanding of the physiological basis of TMS would enable more rational protocols to increase the utility of the technique and accelerate its clinical applications.

Prior studies of TMS-induced changes in cortical excitability included functional brain imaging to identify increased cerebral blood flow in the purported regions of activation[10,11] and at regions distant from the site of stimulation[11]. Further, biophysical models of the electric fields induced by TMS suggested sites and mechanisms of activation[12–14] and effects on cortical circuits[15]. Several recent studies made direct *in vivo* measurements of the effects of TMS on neuronal activity. Allen et al. performed TMS in visual cortex of anesthetized cat[16] but encountered large TMS-generated stimulation artifacts that precluded neuronal recording during TMS. Their analysis of neural activity tens to hundreds of seconds after TMS was useful for studying prolonged changes in excitability that occur after repetitive TMS (rTMS), but it did not address how single TMS pulses affect the activity of single neurons. Similarly, Moliadze et al. recorded the long latency effects of TMS on spontaneous and visual-evoked single unit activity in anesthetized cat[17,18]. Both of these studies were limited by the use of large, human-scale coils to deliver TMS, recordings under anesthesia, and stimulation artifacts precluding the recording of short latency direct effects on neurons. A recent *in vivo* study used a mini-coil within the skull-mounted recording chamber of non-human primates and offline signal manipulation to mitigate the stimulus artifact[19]. However, the small size of the round coil is unlikely to produce effects comparable to those of typical human TMS coils at motor threshold, and the electric field of the round coil is maximal under the coil perimeter but is zero under the center of the coil, therefore largely affecting neurons lying near the perimeter of the recording chamber rather than at the recording site under the center of the coil[19].

Here we describe innovative methods to deliver TMS in alert non-human primates during simultaneous recordings of single neuron activity within 1 ms following the TMS pulse. We developed a novel TMS coil that interfaces directly with a commercially available TMS unit and produces supra-threshold stimulation effects concentrated at the center of a typical skull-mounted recording chamber. We identified, analyzed, and mitigated sources of signal artifacts including large voltage artifacts produced by the TMS pulse that otherwise saturate the recording amplifiers, currents induced in the recording leads and electrode that could cause inadvertent electrical stimulation of the recorded neuron(s), and vibrations generated by coil expansion that obscure short latency neuronal activity. These innovations allow direct recording of single unit neural activity minimally perturbed by stimulation artifact at the site of peak stimulus strength in intact, alert macaques, and enable studies critical to advance and optimize the application of TMS.

NIH-PA Author Manuscript

NIH-PA Author Manuscript

NIH-PA Author Manuscript

RESULTS

Stimulation coil

The design objectives for the TMS coil were to enable it to be used in conjunction with a standard cranial implant for experiments in behaving non-human primates, to induce an electric field within the core of the electrode chamber (i.e., where the tips of recording microelectrodes would be positioned), to generate an electric field with intensity sufficient to evoke a motor response (as proportions of motor threshold are typically used to set the intensity of TMS), and to manage appropriately the thermal and mechanical loads that result from passing large currents through small coils. It is desirable that the TMS coil be comparable or smaller in size than the target brain for increased focality; a consequent challenge is that smaller coils are subject to greater thermal and mechanical stresses[20].

A conventional butterfly coil uses two adjacent coil windings with current in opposite directions to induce a strong, focal electric field where the two windings are closest[21]. This principle was employed to develop a two-winged butterfly coil with the two halves of the coil separated to induce peak electric field strength at the site of the chamber (Supplementary Fig. 1). The rhesus macaques in the present work were implanted with non-ferrous recording chambers (6-ICO-J0, Crist Instruments) secured with dental acrylic and ceramic bone screws (SA45, Thomas Recording). The recording chamber had an outer diameter of 3 cm, imposing a constraint on stimulation coil designs. Another consideration was the non-ferrous head post (6-FHP-J1, Crist), typically positioned at the apex of a cranial implant, which limits placement of the TMS coil.

Finite element models of the TMS coils and a 7 cm diameter sphere approximating a macaque head were constructed in MagNet (Infolytica, Montreal) to evaluate modifications to increase the strength and focality of the induced electric field (Fig. 1a – i). Neural activation thresholds for the models were derived from available human motor threshold data and the electrical characteristics of the modeled stimulation coil (Online Methods). Simulations guided revisions to the coil design for increased electric field strength at the center of the coil, including changing the winding geometry into a “D” shape and tilting the wings down 30° from the horizontal. The resulting coil produced supra-threshold field intensities to a depth of 16 mm from the surface of the head in the model, and given the ~10 mm thickness of dental acrylic plus skull and tissue, this corresponds to ~6 mm below the brain surface. The motor threshold is the lowest intensity that yields an observable, projection-neuron driven output, but below this threshold (i.e., deeper into the brain) other neuronal elements and circuits could be activated. Electric field measurements in a round bottom flask of normal saline approximating the macaque head revealed excellent agreement with the results of the finite element model (Fig. 1j–o). We used fiberglass reinforcement to maintain the structural integrity of the braided litz wire coil, polyimide tape for extra insulation, and thermally conductive epoxy and thermal grease for heat management.

Measurements were taken to evaluate the structural, thermal, and electrical performance of the final cool compared to a standard human coil (Supplementary Fig. 2 and 3). To analyze stresses experienced by the coil, we performed a two-dimensional structural analysis using the finite element method. The modeling was conducted in Multiphysics (COMSOL) to

NIH-PA Author Manuscript

NIH-PA Author Manuscript

NIH-PA Author Manuscript

estimate the maximum stresses in the potting material, using the peak force of a round coil approximating the outline of the wings of the chamber centric coil and the mechanical properties of the cured thermally conductive epoxy. Although the stresses in the model were below the yield stress of the potting compound (18.85 MPa; Supplementary Fig. 2), woven fiberglass cloth (Bondo 499 fiberglass cloth, 3M) was embedded within the potting in the final design to provide a mechanical safety factor. The coil was potted with a thermally conductive epoxy (832TC, MG Chemicals) to provide mechanical support of coil windings and to dissipate heat produced by the coils during use. Coil windings consisted of braided litz wire (48636SN Type 7, Cooner Wire) chosen for availability, flexibility during coil winding, reduced high-frequency losses, and as a compromise between wire dimensions and wire resistance. Additional precautions incorporated during coil construction included the use of polyimide film tape (1205 tape, 3M) applied to one side of the litz wire for insulation between the layers of the coil windings, and to insulate wires close to the surface of the coil mold. Thermal grease (Tgrease 1500, Laird Technologies) was also included during winding of the coils to fill in any air pockets that could insulate the wiring from the thermally conductive epoxy. Once constructed, the coil was tested to ensure that it could withstand the repetitive forces of TMS and that coil heating was well managed (Supplementary Fig. 3a). The time courses of the current through the chamber centric coil (Supplementary Fig. 3b) and the electric field it induced (Supplementary Fig. 3c) were comparable to those of a standard Magstim butterfly coil, albeit slightly lower in magnitude and longer in duration.

Electrophysiology recording equipment

Application of the TMS pulse generates a large voltage artifact in electrical recordings that causes amplifier saturation and filter ringing, which obscure and distort neuronal signals for tens of milliseconds or more. We modified a BAK Electronics Model A-1 recording system, consisting of a remote headstage probe and a rack mounted amplifier, to function in the presence of the large artifacts and enable recording of neuronal activity within 1 ms after the stimulus pulse.

Voltage artifact reduction—The initial mitigation of TMS artifacts was via diodes to clip the artifact, combined with serial low gain amplification, such that the clipped artifact did not cause amplifier saturation (Fig. 2a). After the initial front-end of the headstage, which was unmodified to preserve the high input impedance, two low leakage diodes (BAS45A) were connected anti-parallel between the signal lines and ground before each stage of amplification. Diode clamping resulted in a squarewave-shaped artifact that generated significant post-stimulus ringing that interfered with the neuronal signal. The recording system included Butterworth filters intended to reduce noise generated by an eye coil tracking system (typical for *in vivo* primate neurophysiology). However, these filters were underdamped in the time domain and generated substantial ringing in response to clipped stimulus artifacts. The Butterworth filters were replaced with Bessel filters, which exhibit an overdamped step response, and this eliminated the ringing in response to the stimulation artifacts.

Although the diodes prevented amplifier saturation, the immediate post-stimulus signal remained distorted by the artifact at high stimulation intensities. To reduce the artifact

NIH-PA Author Manuscript

NIH-PA Author Manuscript

NIH-PA Author Manuscript

further, we developed a hardware-based artifact subtraction approach (Fig. 2b) similar to interference compensation in simultaneous electrophysiological recordings and magnetic resonance imaging[22]. The artifact waveform was detected via induction in an external pickup coil positioned next to the stimulation coil, and following scaling, was subtracted from the recorded signal to remove the stimulation artifact. The two signal lines were summed after the initial front-end amplification to preserve the input properties. The small residual artifact that remained after subtraction was clipped by the diodes during subsequent amplification, and was useful as a clear time-stamp of TMS application in the neuronal signal trace. The end result was an artifact subtraction method that resulted in no distortion of the post stimulus signal as compared to diode clamping alone (Fig. 2c–e). This hardware was used in the recording experiments described below.

Current induced in recording leads—The rapidly changing magnetic field generated by TMS can induce electric currents through the recording leads due to the changing magnetic flux through wire loops formed with the electrical recording leads (Supplementary Fig. 4). Induced current through the recording electrode as small as 1 μA could result in direct neuronal activation[23] and obscure determination of the effects of TMS on neurons. This effect was not considered in prior studies of TMS effects on neurons[16–19]. Therefore we performed theoretical calculations and empirical measurements, both *in vitro* and *in vivo*, of the electrode-mediated, induced current (Online Methods).

The theoretical induced current was estimated to be 76 nA, and experimental measurements confirmed that induced currents were unlikely to ever exceed 0.5 μA even at 100% stimulator output. Altogether, the calculations and measurements indicate that, in our setup, the induced currents in the recording leads due to the time varying magnetic field produced by TMS are not large enough to alter neural activity, and that any neuronal activity measured by the recording leads is due solely to the effects of magnetic stimulation via induction in the neuronal tissue.

Artifacts resulting from vibration

Initial *in vivo* neuronal recordings using the instrumentation described above resulted in unexpected post-stimulus artifacts lasting several milliseconds beyond the sub-millisecond TMS artifact (Fig. 3a). These artifacts were determined to be mechanical in origin due to their consistency across changes in the settings of the recording electronics and dependence on stimulation intensity. Further testing, in which the mechanical coupling was varied between the TMS coil and recording setup, verified that these artifacts were indeed mechanical. The large magnetic field produced during TMS results in movement of the copper wire windings of the TMS coils, producing audible clicks and vibration of the TMS coil.

The mounting of the TMS coil to the experimental rig was modified to minimize vibrations. Plastic nuts were embedded in the molded TMS coil to enable connection to an articulating arm (Fisso 3D articulated arm, model 14849, Baitella AG). The articulating arm was mounted to the primate chair using an isolation mount (V11Z51MFRB030, Advanced Antivibration Components). Further, the relative movement between the two electrical

NIH-PA Author Manuscript

NIH-PA Author Manuscript

NIH-PA Author Manuscript

recording points, the reference guide tube and the metal microelectrode, was reduced by insertion of intervening polyimide tubing (TWPT-0100-30–50, Small Parts). These changes reduced the amplitude of the artifact due to vibration to ≤ 15 μV, allowing observation of neuronal activity immediately following the electrical TMS artifact (Fig. 3b). Additional artifact reduction was possible offline with template subtraction, in which the signal averaged over multiple TMS pulses at points in an electrode penetration with no elicited neural activity was subtracted from subsequent data (Fig. 3c). To verify that this template includes no evoked spikes, one must inspect the artifact waveform over several hundred μm of depth, a range in which short-latency, time-locked action potentials should be visible as deflections that drop in and out. Using these vibration-mitigating techniques and the modified recording electronics, the total artifact duration due to TMS, during which neuronal signals could not be resolved, was about 0.7 ms, or only slightly longer than the 0.4 ms duration TMS pulse.

Additional considerations

A number of additional issues should be considered when applying these methods. First, the intensity of the electric field induced by TMS decreases with distance from the coil, making it important to place TMS coils as close as possible to the target tissue. During a typical cranial implant, dental acrylic is applied generously to secure the recording chamber, as there is little downside to increasing the thickness of the acrylic. But in the context of applying TMS, excess thickness can result in an increased offset of the TMS coil from the neural tissue, and unevenly applied or oddly molded acrylic can make it difficult to place the coil against the recording chamber. In such cases, if TMS is to be used on an animal not expressly prepared for such stimulation, excess acrylic should be drilled to form a thinner, more even surface. In animals prepared expressly for combined TMS/recording experiments, the acrylic should be applied conservatively; it helps to have a TMS coil in surgery to verify that the result will allow close proximity between the coil and the skull with minimal intervening acrylic. Additionally, the coil requires space vertically along the recording chamber, necessitating our use of a chamber extension (built in-house of CILUX, similar to 6-YNP-J3, Crist) to allow the micro-drive to be mounted above the stimulation coil.

A second concern is the loud clicking produced by the mechanical deformation of the stimulation coil during TMS. The high intensity click can cause permanent hearing damage in experimental animals, which can be avoided with the use of protective earplugs[24]. The peak sound pressure from our final custom TMS coil was 135 dB 10 cm from the coil, within the damage risk range of 110–140 dB[24]. Depending on the orientation of the TMS coil to the recording chamber, one wing of the coil may be located directly over the ear of the macaque, resulting in even greater sound pressure levels at the eardrum. In addition to hearing damage, the animal may exhibit a startle reflex likely related to the perception of the click even when protective earplugs are used. Also, there is the possibility of muscle activation in the remaining scalp musculature around the cranial implant. Monkeys must be given time to acclimate to such disturbances; we found that typically a week or two of exposure to the procedure is needed before the animal is used to the sounds and sensations and exhibits little or no reaction to them.

NIH-PA Author Manuscript

NIH-PA Author Manuscript

NIH-PA Author Manuscript

The use of a sham control in studies using TMS ensures that observations made during experimentation are not due solely to the auditory stimulus or scalp sensation. Comparing sham to test TMS allows one to isolate effects that are due solely to the TMS-induced intracranial electric field. To create a sham TMS condition, we developed, implemented, and validated a switching scheme to reverse the current direction in one wing of our butterfly shaped coil[25]. Thus, the electric fields induced by each half of the coil were opposite in sign and canceled each other under the center of the coil. Due to minimized interruption and absence of a change in coil placement, this approach was superior to the alternative of physically replacing the stimulation coil with a second, sham coil during the course of an experiment. The simulation results and empirical data on the electric field strengths produced by switching the coil from active mode to sham mode are shown in Fig. 1.

Simultaneous magnetic stimulation and neuronal recording

Our techniques allowed for reliable measurement of single neuron responses over long recording sessions (90 minutes or longer) with high intensity TMS, enabling the investigation of single pulse TMS effects on neuronal activity. Examples of neuronal responses immediately following active and sham TMS at the same recording site are shown in Fig. 4a. TMS pulses were spaced 12 seconds apart (0.083 Hz) to mitigate possible lasting (rTMS) effects between pulses[26]. TMS pulses elicited the activation of a variety of neuronal elements including putative axons, inhibitory neurons, and excitatory (pyramidal) neurons (Fig. 4a). Note that action potentials were resolved within 1 ms of TMS pulse onset (which is at time zero on all plots). Matched sham TMS pulses elicited similar artifacts but no activation (Fig. 4a). For each cortical site tested with TMS, we used cluster cutting (PCA) techniques to identify action potential waveforms produced by individual neuronal elements and plotted rasters of their spiking times; an example is shown in Fig. 4b. The average action potential waveform (±s.e.m.) for this neuron is shown at lower right. The time scale is longer here than in Fig. 4a, and spontaneous activity is appreciable, so low-frequency spiking is evident throughout the recordings in both active and sham conditions (12 trials each). Before active TMS (time < 0) the average activity was 5.0 spikes/s, before sham TMS (bottom, time < 0) it was 7.8 spikes/s, and after sham TMS (time > 0) it was 4.4 spikes/s. After active TMS, however (time > 0), the activity increased significantly to 25.0 spikes/s (Kruskal-Wallis test on trial-by-trial firing rates across the four conditions (before and after active and sham TMS): $p = 0.0004$, $H = 18.48$, $df = 3$). The firing rate after active TMS exceeded the firing rates in all three other conditions (Mann-Whitney U tests corrected for the three comparisons, two-sided $p < 0.0167$ criteria: $p = 0.0003$ vs. before active TMS, $U_A = 9$, $z = 3.61$; $p = 0.0027$ vs. before sham TMS, $U_A = 19.5$, $z = 3$; and $p = 0.0002$ vs. after sham TMS, $U_A = 8$, $z = 3.67$). From neuron to neuron, diverse activation patterns were seen, such as short-latency activation followed by a “rebound” burst (Fig. 4c), moderate-latency activation (Fig. 4d), and transient inhibition (Fig. 4e).

Averaged across neurons, the population response to active TMS was an increase in activity that lasted ~100 ms or longer, as illustrated for a site in the frontal eye field that we tested repeatedly over five days (Fig. 5a). Effects of TMS were measured at this site as a function of both intensity and active/sham configuration. We analyzed changes in firing rate after TMS by calculating the average baseline firing rate (over the 500 ms period before each

NIH-PA Author Manuscript

NIH-PA Author Manuscript

NIH-PA Author Manuscript

TMS pulse) and subtracting that value from the spike density functions of raw firing rates[27]. The data were then averaged across neurons. We found that the population response to active TMS reached nearly 20 spikes/s above baseline for high intensity stimulation (90% level) but stayed near baseline for low intensity stimulation (10% or 50% levels). Analyzed over the approximate response period at this site (0–200 ms after TMS; Fig. 5b), there was a significant difference in the population response to TMS across the four conditions (Kruskal-Wallis test: $p = 0.0032$, $H = 13.8$, $df = 3$). In pairwise comparisons (Mann-Whitney U tests, two-sided $p < .025$ criteria because each sample was compared twice), the response to high intensity active TMS exceeded the response to both low intensity active TMS ($p = 0.0031$, $U_A = 104$, $z = 2.96$; i.e., dose effect) and high intensity sham TMS ($p = 0.0203$, $U_A = 3$, $z = 2.32$; i.e., coil configuration effect). There were no significant differences, however, between responses to high and low intensity for sham TMS ($p = 0.418$, $U_A = 81$, $z = 0.81$; no dose effect) or to active and sham TMS at low intensity ($p = 0.254$, $U_A = 253$, $z = 1.14$; no coil configuration effect). These neural recording data provide robust proof-of-principle evidence that our approach is capable of determining how single pulses of TMS affect neuronal elements in the primate brain.

DISCUSSION

Our novel methods to mitigate artifacts during high-amplitude TMS allow direct observation of its effects on single unit neural activity using the full range of stimulation levels available from a commercial TMS device, a range comparable to that used in human TMS. Moreover, our standardized hardware is compatible with previously prepared animal models without the need for further surgery or significant modifications. This approach greatly reduces the barrier to using TMS as a tool in the non-human primate electrophysiology laboratory.

We encountered three main sources of artifact when developing these methods: large induced voltages, induced currents in the recording electrode, and mechanical vibration. All three artifacts were mitigated sufficiently to permit simultaneous neuronal recording. Of the three artifacts, most insidious and worrisome to us was current injection through induction in the recording electrode and the loop formed by its leads. Such current artifacts could cause spurious neuronal activation (essentially, routine electrical stimulation) that could be mistaken for the direct effects of TMS on the brain. We monitored and mitigated the effects to ensure injected currents well below 1 μA. It is extremely doubtful that the residual current introduced by the electrode into the extracellular space surrounding recorded neurons could have caused the neuronal activations that we found. Induced electrode-mediated currents were not addressed in prior studies, and this is a potential caveat in interpreting the results of those experiments[16–19]. The methods for artifact mitigation described here are useful not only for TMS experiments, but also potentially for any current or future method that involves single neuron recording in the presence of electromagnetic and vibrational disturbances.

The successful neuronal recordings during TMS, representing initial experiments with our custom TMS coil and modified recording system, illustrate the utility and power of the methods. They are just the beginning, however, of possible investigations using simultaneous TMS and neural recordings in animal models. These methods may also have

NIH-PA Author Manuscript

NIH-PA Author Manuscript

NIH-PA Author Manuscript

utility in recording local field potentials (LFPs), which provide low-frequency information about neural activity that is complementary to single unit action potential recordings[28]. Analogously, experiments that record the electroencephalogram (EEG) have been valuable for studying the effects of TMS on evoked and ongoing activity of neuronal populations in humans[29,30]. A number of questions in neuroscience can be explored using trained animals while applying TMS and determining how its effects on behavior correlate with concomitant effects on neuronal activity. Such experiments could shed light on the neuronal mechanisms of TMS to expand knowledge on the workings of the brain in general, and, most importantly, to guide and optimize future clinical applications of TMS. Despite the large volume of work done with TMS, there is little knowledge concerning its effects on neurons. By combining TMS with conventional electrophysiology, the ability to study the mechanisms of TMS is vastly expanded, and is key to research and development that is needed to usher in the next generation of noninvasive TMS technologies and treatments.

ONLINE METHODS

Finite element modeling

The methods for constructing finite element models of spherical heads and TMS coils are detailed in previous work[32]. In brief, a 7 cm diameter sphere approximating the rhesus macaque head was drawn in MagNet 7 (Infolytica Corp., Montreal, Canada) and was assigned isotropic conductivity corresponding to gray matter. The TMS coil designs were drawn above the head model and assigned electrical characteristics based on the conductive wire. A sinusoidal current based on the output of the TMS unit was specified to flow through the coils and the induced electric field in the spherical head model due to the current in the coils was solved.

Estimates of neural activation threshold

The methods for estimating the electric field neural activation threshold are detailed in previous work[32]. In brief, the neural activation threshold, E_{th2}, of the experimental coil with waveform $\omega_2(t)$, was estimated by comparison to known threshold electric field E_{th1} for a coil with electric field waveform $\omega_1(t)$ according to the following:

$$\frac{E_{th1}}{E_{th2}}=\frac{max(|(\omega_2*h)(t)|)}{max(|(\omega_1*h)(t)|)}\,where\,h(t)=\frac{1}{\tau_m}e^{-t/\tau_m}u(t)$$

The convolution operator is represented by *, $h(t)$ is the impulse response of a low pass filter with time constant τ_m= 150 μs[33,34] used to approximate the axonal membrane dynamics, and $u(t)$ is the unit step function. Thus $(\omega*h)(t)$ is proportional to the axonal membrane depolarization due to TMS, and estimates for the electric field thresholds for neuronal membrane firing of the experimental coil (E_{th2}) can be calculated.

Structural analysis

Using the design parameters of the coil and the current from the corresponding electrical circuit model, an estimate of the peak radial force was calculated from the peak current in

NIH-PA Author Manuscript

NIH-PA Author Manuscript

NIH-PA Author Manuscript

the stimulation coil I_{max}, permeability of free space μ_o, number of turns of wire N, coil radius a, and wire radius r using the following expression[21]:

$$F=\frac{1}{2}I_{max}^2\mu_0N^2\left[\ln\left(\frac{8a}{r}-1\right)\right]$$

The estimate of peak radial force during stimulation was coupled with a structural model of the potting material to ensure that it will not fail during use. As the design of the stimulation coil was symmetric, half of the coil was modeled and the displacement perpendicular to the axis of symmetry was fixed to zero (right borders in panels of Supplementary Fig. 2). For increased simplicity the coil was drawn as a planar profile with a specified thickness. The round interior boundary in Supplementary Fig. 2a is where the peak radial force estimate is applied. The resultant peak stress in the model was compared to the strength of the cured potting compound.

The peak force in designs that incorporated non-circular coil windings was approximated using the above equation and a circular radius approximating the coil winding geometry. These same methods were also used in the structural modeling of stimulation coil designs that were no longer planar, however the shortcomings of the simplified model should be kept in mind and extra factors of safety incorporated during the design of the stimulation coil.

Electric field measurements

Electric field measurements were taken using a dipole probe[20] to verify the induced electric field calculated using the models. A round bottom saline flask (250mL 19/22 round bottom flask, Kontes) with an approximate diameter of 83 mm was filled with normal saline to approximate the macaque head. The dipole probe consisted of two single conductor 24AWG copper wires twisted together, with a separation of 3 mm at the exposed ends. The flask was placed on the TMS coil with the flask neck collinear with the chamber axis of the TMS coil. The probe was moved vertically along the axis to make measurements at various depths from the flask border during stimulation.

Current induced in recording electrode and leads

The magnitude of the electrode-mediated, induced current was estimated by calculating the electromotive force, ε, for a loop of wire of area *A* perfectly coupled to the peak magnetic field *B* of a TMS coil using Faraday's law of induction as shown in (1), where Φ_B is the magnetic flux, and *T* is the magnetic sine pulse period.

$$max|\varepsilon|=max\left|\frac{d\Phi_B}{dt}\right|=\left|\frac{2\pi BA}{T}=\frac{2\pi\times 1.5T\times 6.45cm^2}{0.4ms}=15.2V\right. \quad (1)$$

Treating the headstage dc blocking capacitor as a short and applying Ohm's law to the headstage input resistance of 200 MΩ, the induced current was estimated as ~76 nA. This is considered a worst-case estimate, as the loop created by the recording leads is offset and not perfectly coupled to the area of peak magnetic field from the TMS coil (Supplementary Fig.

NIH-PA Author Manuscript

NIH-PA Author Manuscript

NIH-PA Author Manuscript

4d). Moreover, the leads are twisted together to minimize the effect of the magnetic flux through the area of the wire loop.

To analyze empirically the induced current, the voltage clamping diodes were removed, the gain was minimized so that the electronics did not saturate during TMS, and the recording equipment was set up similarly as during the *in vivo* experiments. The voltages measured with a recording electrode and guide tube in a round bottom saline flask approximating the macaque head were converted to induced current using the headstage input impedance. This method assumes that no current flows into the headstage input and that the only induction loop consists of the electrode, dc blocking capacitor, grounded guide tube, and saline (Supplementary Fig. 5a). These measurements revealed an induced current of approximately 4 nA at 100% stimulator output (Supplementary Fig. 5b), well below a level expected to elicit action potentials in neural elements.

To verify further the previous sub-threshold induced current measurements, the voltage across a shunt resistor was measured to determine the current flowing through the recording leads when connected to an electrode and guide tube located in a round bottom saline flask (Supplementary Fig. 5c). These measurements were particularly challenging to perform due to the sensitivity of the induced electromotive force to modifications of the recording leads, and the sensitivity of the test equipment to the strong magnetic fields produced by TMS. As the electromotive force is proportional to the rate of change of the magnetic field times the area of the induction loop, precautions were taken during these measurements to minimize magnetic field exposure of the test equipment and inductive loop areas. Specifically, measurements of the current through a shunt resistor were made approximately 5 feet from the TMS coil, measurement leads were shielded using high permeability cylinders (MuShield), and the inductive loop area made by the test leads was minimized. Disregarding the brief capacitive spikes at the beginning, middle, and end of the TMS waveforms, due to direct capacitive coupling between the TMS coil and saline (V_{tms} and C_{tms} in the schematic of Supplementary Fig. 5c), the measured induced currents in the electrode lead during TMS of the saline flask were approximately 140 nA and 270 nA at 25% and 50% stimulator output, respectively (Supplementary Fig. 5d). Comparable currents were also measured in the ground lead connected to the saline flask during TMS. The brief capacitive spikes of approximately 10 μs can be disregarded due to their extremely brief duration compared to chronaxies of approximately 120 μs[33,34], suggesting that the capacitive spikes would have minimal effect on neuronal membrane polarization.

As well, measurements through a shunt resistor were repeated with the headstage connected to a recording electrode *in vivo*, using similar precautions to minimize currents induced in the measurement leads. These measurements yielded induced currents in the recording electrode lead of approximately 50 nA and 100 nA at 25% and 50% stimulator output, respectively.

A similar calculation as earlier can be used to obtain an estimate of the induced current in the grounding electrode. The standard human body model for electric discharge is 100 pF in series with 1.5 kΩ. At the dominant frequency of TMS (2.5 kHz) the capacitance dominates the impedance. Assuming the effective capacitance is ten times smaller for the monkey

NIH-PA Author Manuscript

NIH-PA Author Manuscript

NIH-PA Author Manuscript

(10 pF) due to its size relative to humans, yields a reactance of 6.4 MΩΩ. Using the estimate of electromotive force from Equation 1 and Ohm's law, a worst-case current estimate of 2.4 μA is achieved. Again, this is considered a worst-case estimate, as the loop created by the recording leads is offset, minimized, and not perfectly coupled to the area of peak magnetic field from the TMS coil.

Measurement of the current in the ground lead of the *in vivo* preparation was significantly more challenging, likely due to the large area of the inductive ground loops, the possibility of multiple loops through the ground lead, and the low impedance of ground connections (Supplementary Fig. 5c). Using the same methods and equipment as the *in vivo* measurements of current in the recording electrode lead, an initial current of 20 μA at 25% stimulator intensity was obtained. Following extensive additional shielding of test leads and equipment, and twisting of test leads, the measured current in the ground lead was reduced to 1.2 μA at 100% stimulator intensity, and is still likely much lower due to the alterations of the headstage from connecting the shunt resistor and test leads, which are not present during actual experiments.

Monkey neurophysiology

Two rhesus monkeys (*Macaca mulatta*, one 11 year old male and one 15 year old female) were prepared for combined TMS stimulation and single neuron recording in an aseptic surgical procedure in which a craniotomy was made over the region of interest (frontal eye field in prefrontal cortex, centered at +23 A and 20 L), a sterile recording chamber (Crist Instruments) was positioned over it, ceramic bone screws were implanted in the skull (Thomas Recording), and these items in addition to a headpost for restraining the head during experiments were bound with dental acrylic to form an implant. The two monkeys were pair-housed, when compatible matches were available, in a diurnal-cycle room (lights on from 7 a.m. to 7 p.m.) that contained an average of 10 macaques. Both monkeys had been trained to sit in a primate chair and perform visual-oculomotor tasks for neuronal recording studies published previously[35–37] Surgeries were performed at the University of Pittsburgh and Duke University in accordance with the Institute Animal Care and Use Committee at both institutions and in compliance with the guidelines set forth in the United States Public Health Service Guide for the Care and Use of Laboratory Animals.

At the start of a recording session, a 23 gauge, stainless steel guide tube containing a vibration-reducing polyimide tubing insert (Small Parts, Part #TWPT-0100-30–50) was inserted through a plastic grid with 1×1 mm hole spacing[38] (Crist Instruments, Hagerstown, MD) and through the dura to the top of the brain. A single tungsten electrode (500 kΩ to 1 MΩ impedance at 1 kHz; FHC, Bowdoinham, ME) was front-loaded into the guide tube and advanced into the brain using a custom microdrive system (designed by the Laboratory of Sensorimotor Research, NEI, NIH, Bethesda, MD). The frontal eye field was selected as the region of interest because we are experienced at studying it[35–37,39–43] and (relevant to future work) because its location in the arcuate sulcus and its strong activity during visual-motor tasks[44,45] facilitate the study of TMS effects as a function of depth and behavioral state. We established that our recording locations were in the frontal eye field using structural MRI and the physiological criteria of presaccadic eye movement related neuronal activity patterns

NIH-PA Author Manuscript

NIH-PA Author Manuscript

NIH-PA Author Manuscript

and low current thresholds for evoking eye movements with electrical stimulation[42,44,45]. Standard extracellular recording techniques were used to isolate action potentials from single neurons referenced to ground provided by the guide tube (area contacting brain approx. 3 mm^2)[46]. Data collection was controlled using the REX real-time system[47] in parallel with Avex, a custom MS Windows application[48] that collected continuous neuronal waveform data and digitized the traces at a sampling rate of 96 kHz for offline analysis (Fast Track Pro Audio Interface, Avid, Irwindale, CA).

Once the electrode was positioned and ready to record, the custom TMS coil was slid into place around the recording chamber, affixed to the primate chair, and used to deliver single-pulse (0.4 ms duration) biphasic magnetic stimulation at a slow rate (1 pulse/12 sec) at a variety of pulse amplitudes (0–100% of full Magstim Rapid^2 output). All TMS-related findings and associated details are described in Results.

Statistical analyses

All comparisons of neuronal firing rates across conditions were performed with two-sided non-parametric tests. As an initial analysis to determine if firing rates varied significantly across test conditions, the Kruskal-Wallis one-way ANOVA on ranks was used. If that was significant at $p < .05$, pairwise Mann-Whitney U tests were performed using a significance level of $p < .025$, corrected from $p < .05$ because each data set was subjected to two comparisons.

Supplementary Material

Refer to Web version on PubMed Central for supplementary material.

Acknowledgments

This work was supported by a Research Incubator Award from the Duke Institute for Brain Sciences to T.E., M.L.P., M.A.S., and W.M.G. and by NIH grant R21 NS078687 to M.A.S. We thank Cassie Kozyrkov for her assistance with preliminary data collection.

REFERENCES

1. Barker AT. An introduction to the basic principles of magnetic nerve-stimulation J Clin. Neurophysiology. 1991; 8:26–37.
2. Couturier JL. Efficacy of rapid-rate repetitive transcranial magnetic stimulation in the treatment of depression: a systematic review and meta-analysis. J. Psychiatry Neurosci. 2005; 30:83–90. [PubMed: 15798783]
3. Loo CK, Mitchell PB. A review of the efficacy of transcranial magnetic stimulation (TMS) treatment for depression, and current and future strategies to optimize efficacy. J. Affect. Disord. 2005; 88:255–267. [PubMed: 16139895]
4. Martin JL, et al. Repetitive transcranial magnetic stimulation for the treatment of depression - Systematic review, meta-analysis. Br. J. Psychiatry. 2003; 182:480–491. [PubMed: 12777338]
5. Picht T, et al. Preoperative functional mapping for Rolandic brain tumor surgery: Comparison of navigated transcranial magnetic stimulation to direct cortical stimulation. Neurosurgery. 2011; 69:581–588. [PubMed: 21430587]
6. Spellman T, et al. Differential effects of high-dose magnetic seizure therapy and electroconvulsive shock on cognitive function Biol. Psychiatry. 2008; 63:1163–1170.

NIH-PA Author Manuscript

NIH-PA Author Manuscript

NIH-PA Author Manuscript

7. Haraldsson HM, Ferrarelli F, Kalin NH, Tononi G. Transcranial magnetic stimulation in the investigation and treatment of schizophrenia: a review. Schizophr. Res. 2004; 71:1–16. [PubMed: 15374567]
8. Hoogendam JM, Ramakers GMJ, Di Lazzaro V. Physiology of repetitive transcranial magnetic stimulation of the human brain. Brain Stimul. 2010; 3:95–118. [PubMed: 20633438]
9. Wagner T, Valero-Cabre A. & Pascual-Leone, A. Noninvasive human brain stimulation. Annu. Rev. Biomed. Eng. 2007; 9:527–565. [PubMed: 17444810]
10. Fox PT, et al. Column-based model of electric field excitation of cerebral cortex. Hum. Brain Mapp. 2004; 22:1–14. [PubMed: 15083522]
11. Paus T, et al. Transcranial magnetic stimulation during positron emission tomography: A new method for studying connectivity of the human cerebral cortex. J. Neurosci. 1997; 17:3178–3184. [PubMed: 9096152]
12. Radman T, Ramos RL, Brumberg JC, Bikson M. Role of cortical cell type and morphology in subthreshold and suprathreshold uniform electric field stimulation in vitro. Brain Stimul. 2009; 2:215–228. [PubMed: 20161507]
13. Miranda PC, Hallett M, Basser PJ. The electric field induced in the brain by magnetic stimulation: A 3-D finite-element analysis of the effect of tissue heterogeneity and anisotropy. IEEE Trans. Biomed. Eng. 2003; 50:1074–1085. [PubMed: 12943275]
14. Silva S, Basser PJ, Miranda PC. Elucidating the mechanisms and loci of neuronal excitation by transcranial magnetic stimulation using a finite element model of a cortical sulcus. Clin. Neurophysiol. 2008; 119:2405–2413. [PubMed: 18783986]
15. Esser SK, Hill SL, Tononi G. Modeling the effects of transcranial magnetic stimulation on cortical circuits. J. Neurophysiol. 2005; 94:622–639. [PubMed: 15788519]
16. Allen EA, Pasley BN, Duong T, Freeman RD. Transcranial magnetic stimulation elicits coupled neural and hemodynamic consequences. Science. 2007; 317:1918–1921. [PubMed: 17901333]
17. Moliadze V, Giannikopoulos D, Eysel UT, Funke K. Paired-pulse transcranial magnetic stimulation protocol applied to visual cortex of anaesthetized cat: effects on visually evoked single-unit activity. J. Physiol. 2005; 566:955–965. [PubMed: 15919717]
18. Moliadze V, Zhao Y, Eysel U, Funke K. Effect of transcranial magnetic stimulation on single-unit activity in the cat primary visual cortex. J. Physiol. 2003; 553:665–679. [PubMed: 12963791]
19. Tischler H, et al. Mini-coil for magnetic stimulation in the behaving primate. J. Neurosci. Meth. 2011; 194:242–251.
20. Weissman JD, Epstein CM, Davey KR. Magnetic brain-stimulation and brain size - Relevance to animal studies. Electroencephalogr. Clin. Neurophysiol. 1992; 85:215–219. [PubMed: 1376680]
21. Ruohonen, J.; Ilmoniemi, RJin. Handbook of Transcranial Magnetic Stimulation. Pascual-Leone, A.; Davey, NJ.; Rothwell, J., editors. Oxford, UK: Oxford University Press; 2002. p. 18-30.
22. Oeltermann A, Augath MA, Logothetis NK. Simultaneous recording of neuronal signals and functional NMR imaging. Magn Reson Imaging. 2007; 25:760–774. [PubMed: 17478070]
23. Stoney SD, Thompson WD, Asanuma H. Excitation of pyramidal tract cells by intracortical microstimulation: effective extent of stimulating current. J. Neurophysiol. 1968; 31:659–669. [PubMed: 5711137]
24. Counter SA, Borg E, Lofqvist L, Brismar T. Hearing-loss from the acoustic artifact of the coil used in extracranial magnetic stimulation. Neurology. 1990; 40:1159–1162. [PubMed: 2381522]
25. Ruohonen J, Ollikainen M, Nikouline V, Virtanen J, Ilmoniemi RJ. Coil design for real and sham transcranial magnetic stimulation. IEEE Trans. Biomed. Eng. 2000; 47:145–148. [PubMed: 10721620]
26. Chen R, et al. Depression of motor cortex excitability by low-frequency transcranial magnetic stimulation. Neurology. 1997; 48:1398–1403. [PubMed: 9153480]
27. Macpherson JM, Aldridge JW. Quantitative method of computer-analysis of spike train data collected from behaving animals. Brain Res. 1979; 175:183–187. [PubMed: 487149]
28. Buzsáki G, Anastassiou CA, Koch C. The origin of extracellular fields and currents--EEG, ECoG, LFP and spikes. Nat. Rev. Neurosci. 2012; 13:407–420. [PubMed: 22595786]

NIH-PA Author Manuscript

NIH-PA Author Manuscript

NIH-PA Author Manuscript

29. Kähkönen S, Komssi S, Wilenius J, Ilmoniemi RJ. Prefrontal transcranial magnetic stimulation produces intensity-dependent EEG responses in humans. Neuroimage. 2005; 24:955–960. [PubMed: 15670672]
30. Ilmoniemi RJ, Kicić D. Methodology for combined TMS and EEG. Brain Topogr. 2010; 22:233–248. [PubMed: 20012350]
31. Lemon, R. Methods for neuronal recording in conscious animals. Vol. 4. Wiley, Hoboken, NJ: IBRO handbook series; 1984.
32. Deng ZD, Lisanby SH, Peterchev AV. Electric field strength and focality in electroconvulsive therapy and magnetic seizure therapy: a finite element simulation study. J. Neural Eng. 2011; 8:016007. [PubMed: 21248385]
33. Barker AT, Garnham CW, Freeston IL. Magnetic nerve-stimulation - the effect of wave-form on efficiency determination of neural membrane time constants the measurement of stimulator output. Electroencephalogr. Clin. Neurophysiol. 1991; 43(Suppl):227–237.
34. Peterchev AV, Goetz SM, Westin GG, Luber B, Lisanby SH. Pulse width dependence of motor threshold and input-output curve characterized with controllable pulse parameter transcranial magnetic stimulation. Clin. Neurophysiol. 2013; 124:1364–1372. [PubMed: 23434439]
35. Mayo JP, Sommer MA. Neuronal correlates of visual time perception at brief timescales. Proc. Natl. Acad. Sci. U.S.A. 2013; 110:1506–1511. [PubMed: 23297217]
36. Crapse TB, Sommer MA. Frontal eye field neurons assess visual stability across saccades. J. Neurosci. 2012; 32:2835–2845. [PubMed: 22357866]
37. Mayo JP, Sommer MA. Neuronal adaptation caused by sequential visual stimulation in the frontal eye field. J. Neurophysiol. 2008; 100:1923–1935. [PubMed: 18684901]
38. Crist CF, Yamasaki DS, Komatsu H, Wurtz RH. A grid system and a microsyringe for single cell recording. J. Neurosci. Methods. 1988; 26:117–122. [PubMed: 3146006]
39. Shin S, Sommer MA. Division of labor in frontal eye field neurons during presaccadic remapping of visual receptive fields. J. Neurophysiol. 2012; 108:2144–2159. [PubMed: 22815407]
40. Sommer MA, Tehovnik EJ. Reversible inactivation of macaque frontal eye field. Exp. Brain Res. 1997; 116:229–249. [PubMed: 9348123]
41. Sommer MA, Wurtz RH. Frontal eye field neurons orthodromically activated from the superior colliculus. J. Neurophysiol. 1998; 80:3331–3335. [PubMed: 9862927]
42. Sommer MA, Wurtz RH. Composition and topographic organization of signals sent from the frontal eye ffield to the superior colliculus. J Neurophysiol. 2000; 83:1979–2001. [PubMed: 10758109]
43. Sommer MA, Wurtz RH. Frontal eye field sends delay activity related to movement, memory, and vision to the superior colliculus. J. Neurophysiol. 2001; 85:1673–1685. [PubMed: 11287490]
44. Bruce CJ, Goldberg ME. Primate Frontal Eye Fields .1 Single Neurons Discharging before Saccades. J Neurophysiol. 1985; 53:603–635. [PubMed: 3981231]
45. Bruce CJ, Goldberg ME, Bushnell MC, Stanton GB. Primate frontal eye fields .2 Physiological and anatomical correlates of Electrically Evoked Eye-Movements. J. Neurophysiol. 1985; 54:714–734. [PubMed: 4045546]
46. Wurtz, RH.; Sommer, MA. in Methods in Mind. Senior, C.; Russel, Tz; Gazzaniga, M., editors. USA: MIT Press, Cambridge, MA; 2006.
47. Hays AV Jr, Richmond BJ, Optican LM. WESCON Conf Proc. :1–10.
48. Ashmore RC, Sommer MA. Delay activity of saccade-related neurons in the caudal dentate nucleus of the macaque cerebellum. J. Neurophysiol. 2013; 109:2129–2144. [PubMed: 23365182]

NIH-PA Author Manuscript

NIH-PA Author Manuscript

NIH-PA Author Manuscript

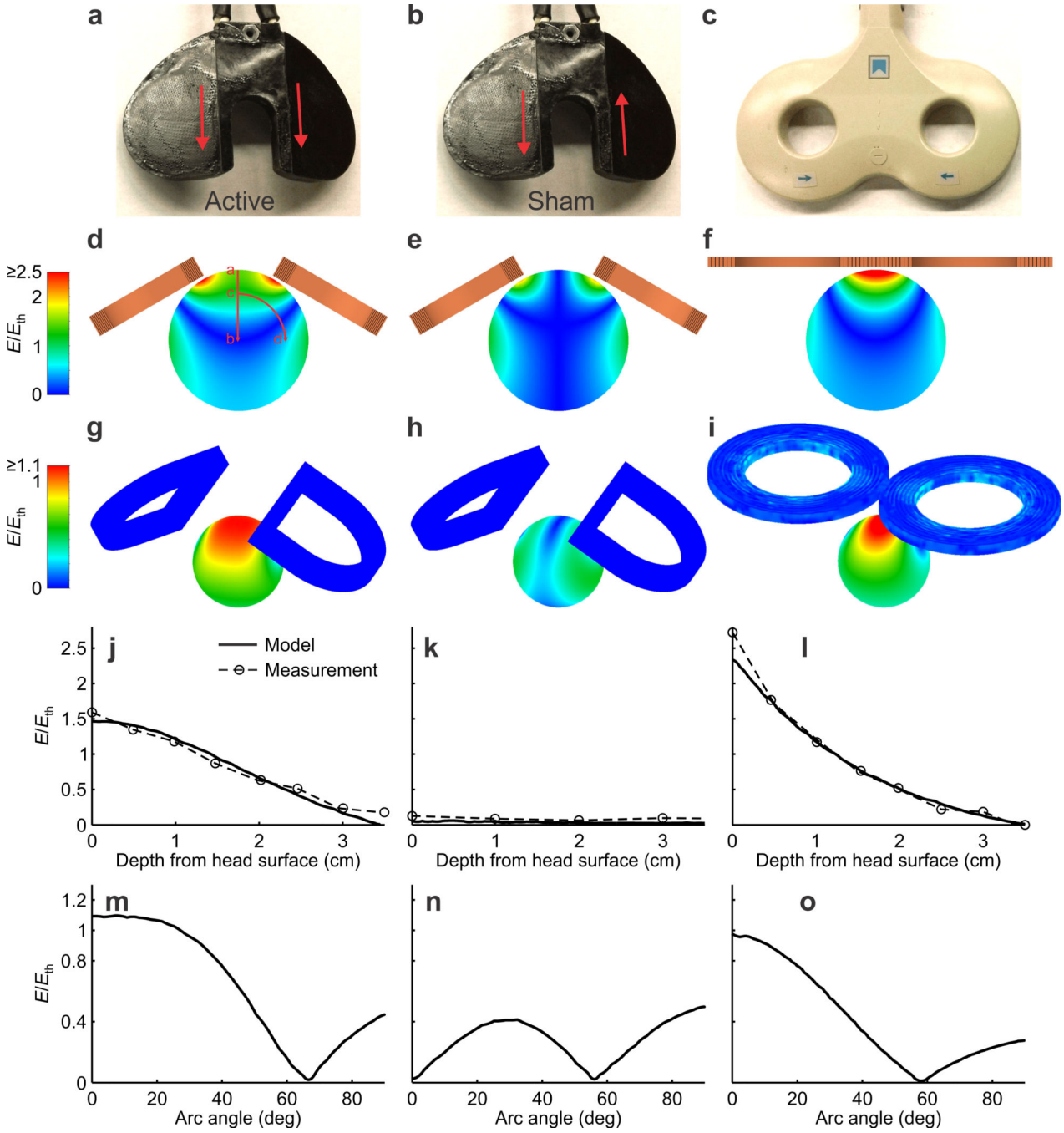

Figure 1.

Models and measurements of the chamber centric coil compared with the Magstim 70 mm butterfly coil at 100% stimulator output (Magstim Rapid^2 base unit). (a) Chamber centric coil in *Active* mode. In this configuration, current directions along the central segments of the coil are parallel, as indicated by the red arrows. (b) Chamber centric coil in *Sham* mode. Current directions along the central segments of the coil are antiparallel. (c) Magstim 70 mm butterfly coil, to scale with the chamber centric coil. In the remaining panels, the three illustrations in each row conform to the coils and modes of (a)-(c), i.e. *left* panel is always

NIH-PA Author Manuscript

NIH-PA Author Manuscript

NIH-PA Author Manuscript

chamber centric active mode, *middle* panel is always chamber centric sham mode, and *right* panel is always the Magstim coil. (d)–(f) Modeled electric field profile, E, normalized to estimated neural activation threshold, E_{th}, through the cross section of the entire sphere that approximates a monkey head. (g)–(i) Same, but shown at the median depth of the recording electrode (2.6 mm below the cortical surface that is modeled as 1 cm below the outer surface of the sphere). (j)–(l) Modeled and measured strength of E relative to E_{th} as a function of depth below the center of the coil, that is, along the line segment $\overline{ab}$ in panel *d*. (m)-(o) Modeled E/E_{th} as a function of angular distance away from the center at the depth of the recording electrode, that is, along the arc $\overline{cd}$ in panel *d*. Measurements were taken in a normal saline filled round bottom flask approximating the sphere.

NIH-PA Author Manuscript

NIH-PA Author Manuscript

NIH-PA Author Manuscript

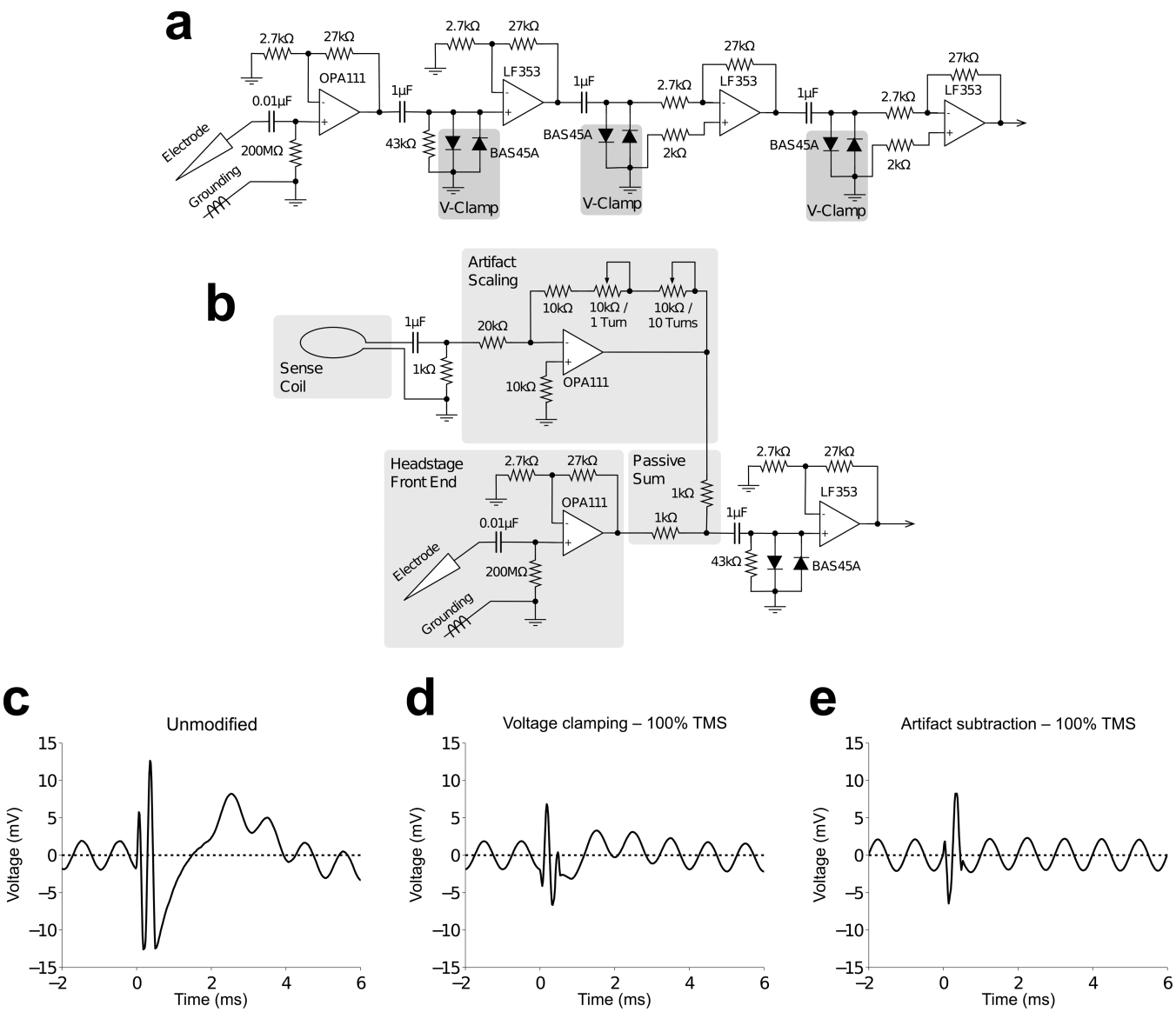

Figure 2.

Voltage artifact reduction strategies. (a) Initial voltage clamping scheme modified from a BAK Electronics Model A-1 recording system. Based on an estimate of maximal neuronal signal amplitude of 100 μV, a gain of 10,000X can be implemented without clipping the neuronal signal, for an amplified neuronal signal of 1 V. (b) Voltage artifact subtraction behind front-end amplifier. A sense coil near the TMS coil generates a similar artifact waveform as that detected in the recording electrode. The sense coil's artifact is scaled such that adding it to the signal from the electrode reduces the TMS artifact dramatically while leaving the neuronal signals unperturbed. The gain and polarity required for artifact scaling is dependent on the size of, and number of turns in, the sense coil, as well as its location and orientation relative to the TMS coil. The use of two rheostats with variable turns functions as separate coarse and fine adjusts for artifact scaling. (c) TMS caused distortion and loss of signal in the unmodified recording electronics immediately following the stimulus pulse. (d) Voltage clamping diodes prevented saturation of recording amplifiers by the TMS artifact,

NIH-PA Author Manuscript

NIH-PA Author Manuscript

NIH-PA Author Manuscript

but the signal immediately following the stimulus pulse was slightly distorted. (e) Subtracting the stimulus artifact induced in a small pickup coil from the composite signal in combination with voltage clamping diodes eliminated the post stimulus distortion. The recorded sinusoid was detected with nearly perfect resolution starting only ~0.5 ms after the onset of stimulus artifact.

NIH-PA Author Manuscript

NIH-PA Author Manuscript

NIH-PA Author Manuscript

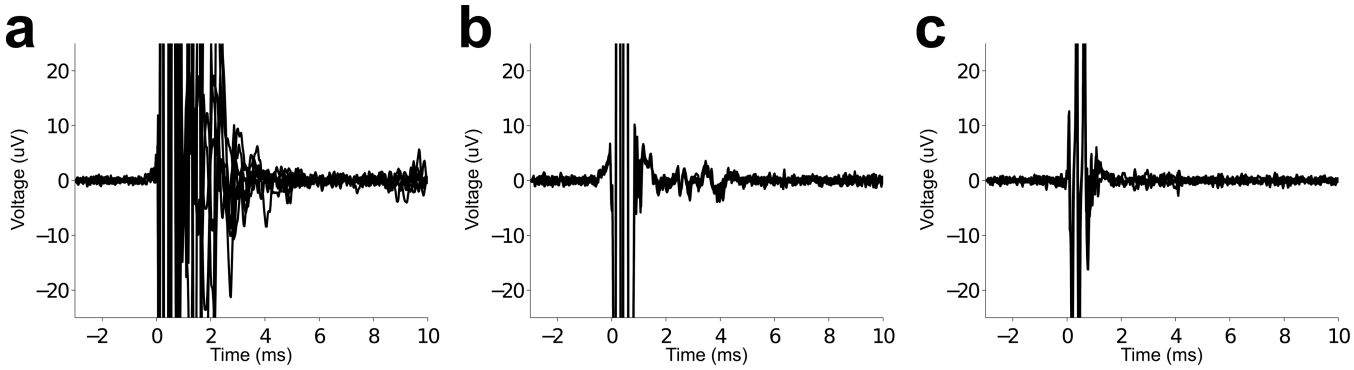

Figure 3.

Examination of mechanical artifacts due to 100% intensity TMS. (a) Voltage recordings made in cerebral cortex without precautions for mechanical artifacts. Overlay of multiple TMS artifacts shows artifacts lasting approximately 4 ms with voltage swings exceeding 100 μV near the electrical TMS artifact and tapering over time. (b) Overlay of TMS artifacts using a modified guide tube with a reduced inner diameter via polyimide tubing. The duration of electrode movement remained about the same as for the regular guide tube, but the amplitude of voltage swings was greatly reduced. Well-isolated neuronal action potentials would project above the minor voltage swings of the mechanical artifact. (c) Offline processing of the minimized artifact by subtracting the average signal reduces post stimulus artifacts further, which would aid observation of neuronal signals 1–2 ms following TMS.

NIH-PA Author Manuscript

NIH-PA Author Manuscript

NIH-PA Author Manuscript

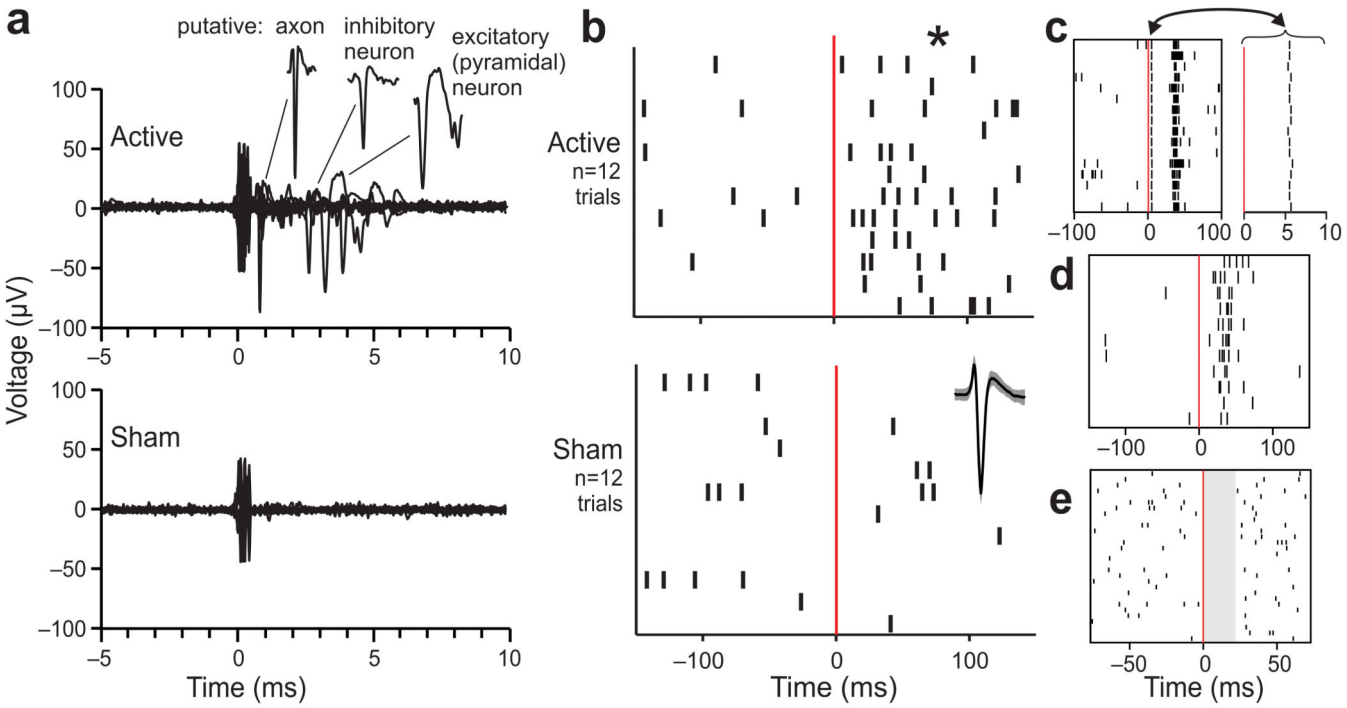

Figure 4.

Recordings of neuronal spikes activated by single pulse TMS. (a) Example raw data from 20 sequential applications of 70% active TMS (*top*) and sham TMS (*bottom*) at the same site in one animal. These data were selected for illustration because the TMS elicited activation of diverse neuronal elements. As shown in the extracted segments (*upper right*), example action potentials included those from a putative axon (very narrow), inhibitory interneuron (broader), and excitatory neuron (very broad)[31]. (b) For quantification, rasters of action potential times relative to active (*top*) and sham (*bottom*) TMS pulses at time zero (red lines) are plotted for an example neuron (its waveform average and ±s.e.m. is shown at right in the sham graph). The neuron was activated significantly by active TMS (*, $p < .01$; see text). (c–e) Examples of TMS-induced activity in three other neurons. The neuron of panel *c* showed short-latency activation (magnified at right for clarity) followed by apparent inhibition and then a burst. The neuron of panel *d* showed no short-latency activation, but had a surge of activity around 20–40 ms latency. The neuron of panel *e* showed clear suppression in activity (shaded) for about 20 ms after TMS. In general, we found that single pulse TMS caused patterns of responses that were reliable for each neuron but diverse between neurons.

NIH-PA Author Manuscript

NIH-PA Author Manuscript

NIH-PA Author Manuscript

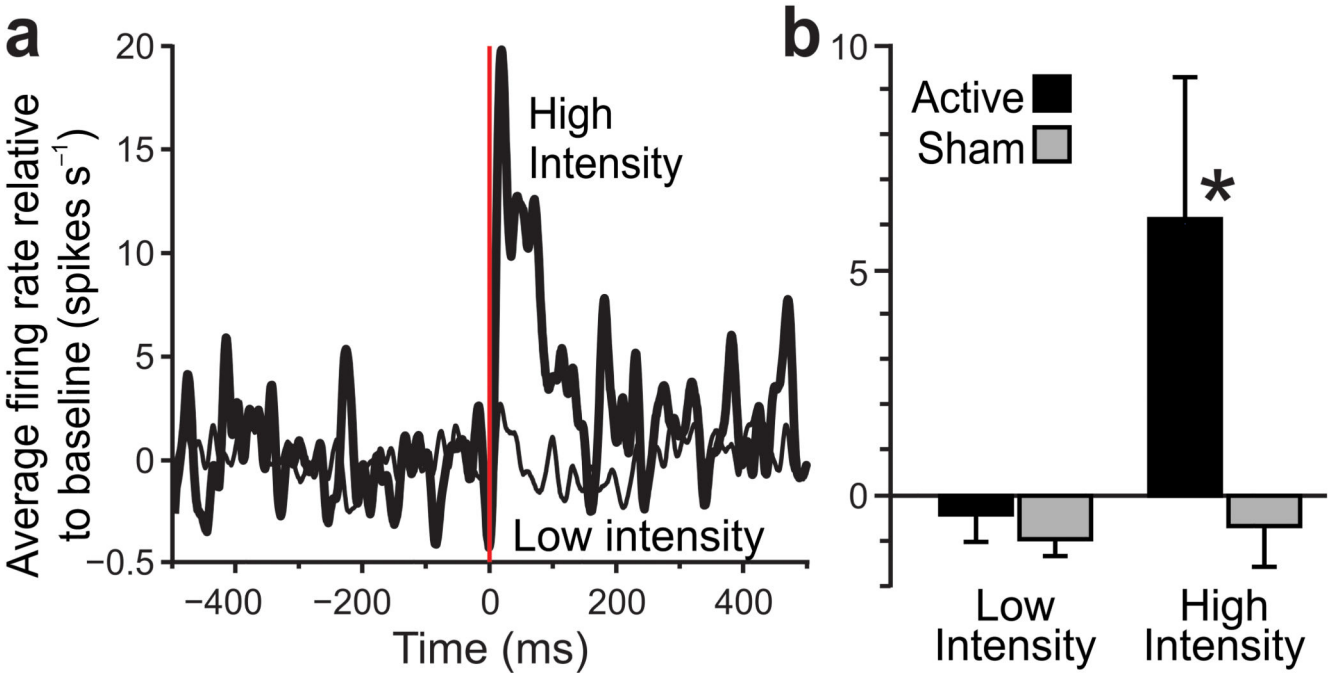

Figure 5.

Population responses to TMS. (a) Time courses of aggregate neuronal activity collected at a site in the frontal eye field where TMS caused predominantly vigorous, excitatory responses, allowing us to analyze the effects of TMS parameters on a population of similar neurons (n = 18 neurons as estimated from action potential analyses; note, one cannot directly visualize and count neurons during *in vivo* monkey experiments). We alternated between active and sham TMS at high intensity (90%, total n = 6 blocks each for active and sham, where one block is 15 repeats at .083 Hz) and low intensity (10–50%, n = 19 blocks for active and 22 blocks for sham). 10% and 50% intensity data were pooled because it was clear that neither level caused activation. The time courses demonstrate that active TMS at high intensity caused a strong response that lasted for ~200 ms, an effect that went away when the intensity was lowered. (b) Quantitatively (each bar shows mean ±s.e.m.), the neuronal response to active TMS at high intensity significantly exceeded (*, $p < .025$) the response to active TMS at low intensity (i.e. dose effect) as well as the response to sham TMS at high intensity (i.e. coil configuration effect). No other comparisons were significant; see text for details.